

University of Groningen

## Electron Capture from Molecular Hydrogen by Metastable Sn<sup>2+</sup>\* Ions

Bijlsma, Klaas; Oltra, Lamberto; Wit, Emiel de; Assink, Luc; Rabadán, Ismanuel; Méndez, Luis; Hoekstra, Ronnie

*Published in:*  
 Atoms

*DOI:*  
[10.3390/atoms12020009](https://doi.org/10.3390/atoms12020009)

**IMPORTANT NOTE:** You are advised to consult the publisher's version (publisher's PDF) if you wish to cite from it. Please check the document version below.

*Document Version*  
 Publisher's PDF, also known as Version of record

*Publication date:*  
 2024

[Link to publication in University of Groningen/UMCG research database](#)

*Citation for published version (APA):*

Bijlsma, K., Oltra, L., Wit, E. D., Assink, L., Rabadán, I., Méndez, L., & Hoekstra, R. (2024). Electron Capture from Molecular Hydrogen by Metastable Sn<sup>2+</sup>\* Ions. *Atoms*, 12(2), Article 9. <https://doi.org/10.3390/atoms12020009>

### Copyright

Other than for strictly personal use, it is not permitted to download or to forward/distribute the text or part of it without the consent of the author(s) and/or copyright holder(s), unless the work is under an open content license (like Creative Commons).

The publication may also be distributed here under the terms of Article 25fa of the Dutch Copyright Act, indicated by the "Taverne" license. More information can be found on the University of Groningen website: <https://www.rug.nl/library/open-access/self-archiving-pure/taverne-amendment>.





### Take-down policy

If you believe that this document breaches copyright please contact us providing details, and we will remove access to the work immediately and investigate your claim.

*Downloaded from the University of Groningen/UMCG research database (Pure): <http://www.rug.nl/research/portal>. For technical reasons the number of authors shown on this cover page is limited to 10 maximum.*

Article

# Electron Capture from Molecular Hydrogen by Metastable $\text{Sn}^{2+*}$ Ions

Klaas Bijlsma <sup>1,2,†</sup> , Lamberto Oltra <sup>3,†</sup> , Emiel de Wit <sup>1,2</sup> , Luc Assink <sup>1,2</sup> , Ismanuel Rabadán <sup>3</sup> , Luis Méndez <sup>3</sup>  and Ronnie Hoekstra <sup>1,2,\*</sup> 

<sup>1</sup> Zernike Institute for Advanced Materials, University of Groningen, Nijenborgh 4, 9747 AG Groningen, The Netherlands

<sup>2</sup> Advanced Research Center for Nanolithography (ARCNL), Science Park 106, 1098 XG Amsterdam, The Netherlands

<sup>3</sup> Laboratorio Asociado al CIEMAT de Física Atómica y Molecular en Plasmas de Fusión, Departamento de Química, Universidad Autónoma de Madrid, Cantoblanco, E-28049 Madrid, Spain

\* Correspondence: r.a.hoekstra@rug.nl

† These authors contributed equally to this work.

**Abstract:** Over a wide and partly overlapping energy range, the single-electron capture cross-sections for collisions of metastable  $\text{Sn}^{2+}$  ( $5s5p\ 3P^o$ ) ( $\text{Sn}^{2+*}$ ) ions with  $\text{H}_2$  molecules were measured (0.1–10 keV) and calculated (0.3–1000 keV). The semi-classical calculations use a close-coupling method on a basis of electronic wavefunctions of the  $(\text{SnH}_2)^{2+}$  system. The experimental cross-sections were extracted from double collisions in a crossed-beam experiment of  $\text{Sn}^{3+}$  with  $\text{H}_2$ . The measured capture cross-sections for  $\text{Sn}^{2+*}$  show good agreement with the calculations between 2 and 10 keV, but increase toward lower energies, whereas the calculations decrease. Additional Landau–Zener calculations were performed and show that the inclusion of spin-orbit splitting cannot explain the large cross-sections at the lowest energies which we now assume to be likely due to vibrational effects in the molecular hydrogen target.

**Keywords:** ion–molecule collisions; electron capture; Sn; molecular hydrogen; EUV source; laser-produced plasma



**Citation:** Bijlsma, K.; Oltra, L.; de Wit, E.; Assink, L.; Rabadán, I.; Méndez, L.; Hoekstra, R. Electron Capture from Molecular Hydrogen by Metastable  $\text{Sn}^{2+*}$  Ions. *Atoms* **2024**, *12*, 9. <https://doi.org/10.3390/atoms12020009>

Academic Editor: Kanti M. Aggarwal

Received: 21 December 2023

Revised: 25 January 2024

Accepted: 29 January 2024

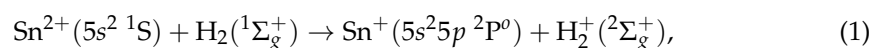
Published: 1 February 2024



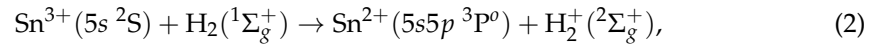
**Copyright:** © 2024 by the authors. Licensee MDPI, Basel, Switzerland. This article is an open access article distributed under the terms and conditions of the Creative Commons Attribution (CC BY) license (<https://creativecommons.org/licenses/by/4.0/>).

## 1. Introduction

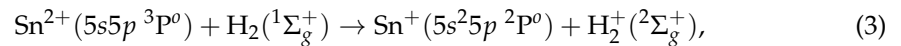
Latest-generation photolithography tools employ a laser-produced plasma (LPP) to generate extreme ultraviolet (EUV) light for writing the smallest features on silicon wafers in the production of computer chips [1–3]. In particular, a dense Sn plasma of about 40 eV in temperature is created in which Sn ions with charge states between 9+ and 15+ are the atomic sources of EUV light at 13.5 nm [4–8]. Energetic Sn ions are emitted from the plasma in lower charge states, typically from 4+ to 8+ [9–11], which is attributed to recombination in the peripheral part of the plasma [12]. To protect the plasma-facing optics from these energetic and highly charged ions, an  $\text{H}_2$  buffer gas is introduced [2,13]. Collisions of the  $\text{Sn}^{q+}$  ions with the  $\text{H}_2$  molecules give rise to one- and two-electron capture reactions stepping down the average charge state of the ions. The initial steps down till  $\text{Sn}^{3+}$  are expected to happen rapidly due to the large cross-sections for the higher charge states [11]. In the whole series of consecutive scattering events while traveling through the buffer gas, the ions' kinetic energy is reduced to values that allow for the efficient mitigation of the Sn ions. Since it seems that the stopping power of  $\text{Sn}^+$  is larger than that of  $\text{Sn}^{2+}$  ions [14], it is key to know whether the charge state lowering stops at 1+ or 2+. Given that the production of singly charged Sn ions by charge exchange from the  $\text{Sn}^{2+}$  ground state, i.e.,



is endothermic with an energy difference of 1.3 eV for the Franck–Condon ionization of  $H_2$  at its equilibrium distance, it has been believed that the consecutive charge state lowering basically stops at 2+. However, in a recent study [11], we have shown that the successive capture reactions do lead to the formation of  $Sn^{2+}$  ions. The work of Rai et al. [11] explains the high production of  $Sn^{2+}$  as a consequence of the preceding single-capture reaction between  $Sn^{3+}$  and  $H_2$ , which was shown [15] to mainly produce long-lived metastable  $Sn^{2+}(5s5p^3P^o)$  ions, i.e.,



and just a very small fraction of ground-state  $Sn^{2+}(5s^2^1S)$  ions. For the metastable  $Sn^{2+}(5s5p^3P^o)$  ions, single-electron capture from  $H_2$ , i.e.,



is not endothermic, but exothermic by 5.8 eV.

To underpin that very long-lived  $Sn^{2+}(5s5p^3P^o)$  metastable ions, later on denoted in short by  $Sn^{2+*}$  ions, are the gateway to produce singly charged Sn ions, Landau–Zener calculations of the capture cross-section of reaction (3) were performed by Rai et al. [11], leading to considerable cross-sections on the order of  $10^{-15} \text{ cm}^2$ . In general, the collision energy at which the Landau–Zener cross-section maximizes depends on the prefactor of the coupling matrix element. The prefactors of Olson and Salop [16] (determined for atomic hydrogen targets) and Kimura et al. [17] (from experiments on He) differ significantly and the associated energies at which the cross-section maximizes differ by a factor of 8. There is no hard objective argument to prefer the H or He prefactor when having molecular hydrogen as a target. In the present work, we therefore present concerted theoretical and experimental efforts to obtain more reliable cross-sections.

We carried out a close-coupling calculation of total cross-sections for reactions (1) and (3) using the method previously applied in [15] for  $Sn^{3+} + H_2$  collisions. At energies which are most relevant for EUV plasma source applications, i.e., below 20 keV, we find that the cross-section for electron capture by  $Sn^{2+*}$  is an order of magnitude larger than the one for ground-state  $Sn^{2+}$ . Experimentally, to prevent issues with not well-known metastable fractions in a  $Sn^{2+}$  ion beam, we performed crossed-beam studies with  $Sn^{3+}$  and  $H_2$ . By looking at double-collision events, we effectively created a crossed-beam experiment of metastable  $Sn^{2+*}$  with  $H_2$ . In this way, we obtained total single-electron capture cross-sections for reaction (3) over the energy range from 0.1 to 10 keV.

## 2. Theoretical Approach

The calculation method has been explained in Ref. [15]. Briefly, we employ a semi-classical treatment with nuclear straight-line trajectories, and the calculation assumes that the H–H internuclear distance is fixed during the collision (Franck–Condon approximation). This method is appropriate for intermediate collision energies. At low energies, the vibrational excitation of  $H_2$  during the collision may be relevant. This effect is not included in the calculation method. At even lower energies, the nuclear motion of the projectile may need to be described with a wavefunction within a quantal formalism. In this respect, previous calculations on electron capture by doubly charged ions ( $O^{2+}$ ,  $N^{2+}$ ) from H, which also involved transitions at avoided crossings at relatively large internuclear distances, showed that the semi-classical method is appropriate for energies higher than about 50 eV/u [18]. Accordingly, we have calculated the cross-sections for  $Sn^{2+*} + H_2$  at energies higher than 5 keV. However, to compare with the experiment and two-state models, we have extended the calculation down to 0.3 keV.

In the semi-classical approximation, the vector position of the ion with respect to the target center of mass,  $\mathbf{R}(t)$ , is a rectilinear trajectory  $\mathbf{R} = \mathbf{b} + \mathbf{v}t$ , where  $\mathbf{b}$  is the impact parameter and  $\mathbf{v}$  the ion–molecule relative velocity. The electronic wavefunction is the solution of the eikonal equation:

$$\left[ H_{\text{el}} - i \frac{\partial}{\partial t} \right] \Psi = 0, \quad (4)$$

where  $H_{\text{el}}$  is the clamped-nuclei non-relativistic electronic Hamiltonian of the quasi-molecule  $(\text{SnH}_2)^{2+}$ . In our treatment, the electronic motion is described by the wavefunction  $\Psi$ , which is expanded in terms of the (approximate) eigenfunctions,  $\chi_k$ , of  $H_{\text{el}}$ :

$$\Psi(\mathbf{r}, t; \mathbf{v}, \mathbf{b}) = D(\mathbf{r}, t) \sum_k c_k(t) \chi_k(\mathbf{r}; \mathbf{R}) \exp\left(-i \int_0^t E_k(\mathbf{R}) dt\right), \quad (5)$$

where  $\mathbf{r}$  are electronic coordinates and  $E_k$  the energies of the electronic wavefunctions  $\chi_k$ . In the present calculation, the wavefunctions  $\chi_k$  were obtained in a multi-reference configuration interaction calculation, with the Gaussian basis set and the pseudo-potential of the calculation of Ref. [15] for  $(\text{SnH}_2)^{3+}$ . The electronic wavefunctions were multiplied by a common translation factor,  $D$  [19], to ensure that the wavefunction (5) fulfilled the initial condition.

In practice, to calculate the total cross-sections for the processes (1) and (3), we employed basis sets of three and six molecular electronic states, respectively, as seen in Figure 1. Due to the conservation of the total spin, both cases were run in independent calculations. For both systems, the basis includes the electronic states dissociating into  $\text{Sn}^{2+}(5s^2\ ^1S) + \text{H}_2(X^1\Sigma_g^+)$  and  $\text{Sn}^{2+}(5s5p\ ^3P^o) + \text{H}_2(X^1\Sigma_g^+)$ , which correspond to the entrance channels of collisions (1) and (3), respectively. The basis set also includes the molecular states dissociating into  $\text{Sn}^+(5s^25p\ ^2P^o) + \text{H}_2^+(X^2\Sigma_g^+)$  and  $\text{Sn}^+(5s5p^2\ ^4P) + \text{H}_2^+(X^2\Sigma_g^+)$ , the main capture channels, and the electronic state that correlates to  $\text{Sn}^{2+}(5s^2\ ^1S) + \text{H}_2(^3\Sigma_u^+)$ , which leads to dissociative excitation.

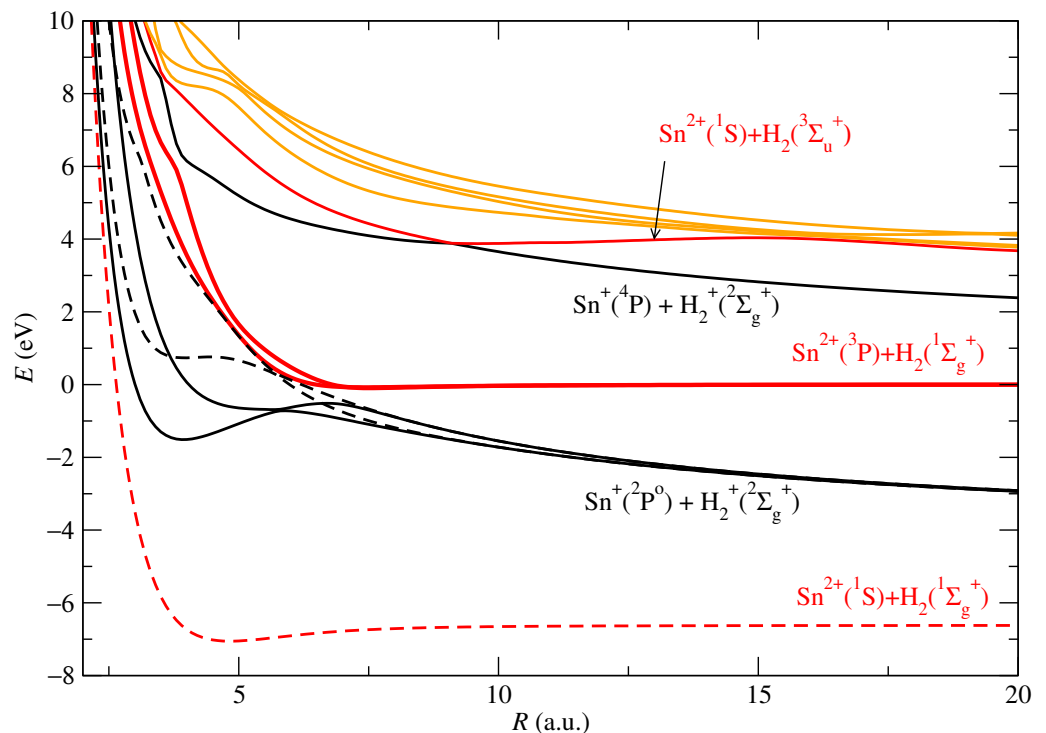


**Figure 1.** Potential energy curves of the  $(\text{SnH}_2)^{2+}$  system as functions of the distance of the Sn nucleus to the midpoint of the H–H internuclear axis. The red lines are the energies of the electronic states correlating to  $\text{Sn}^{2+} + \text{H}_2$ . The black lines represent the energy curves of the states dissociating into  $\text{Sn}^+ + \text{H}_2^+$ . The orange lines are the energies of other states not included in the dynamical calculation. Solid and dashed lines correspond to triplet and singlet subsystems, respectively.

To evaluate orientation-averaged cross-sections, we consider ion trajectories with different orientations ( $\hat{b}, \hat{v}$ ) with respect to the H<sub>2</sub> internuclear axis. As explained in previous works, for ion collisions with H<sub>2</sub>, the symmetry of the molecular target allows us to perform the orientation-average with three trajectory orientations [20]. In the first one (t1), the ion velocity is parallel to the H–H internuclear axis; for the second one (t2), the impact parameter is along the H–H internuclear axis; and the third one (t3) has both the impact parameter and the velocity perpendicular to the H–H internuclear axis. For each orientation, and for each value of the impact parameter, we substitute the expansion (5) into the eikonal equation, which yields a system of first-order differential equations for the coefficients  $c_k$ . They are solved with the initial condition  $c_k(t = -\infty) = \delta_{ik}$ , where the index  $i$  corresponds to the collision entrance channel. The populations of the different electronic states of (SnH<sub>2</sub>)<sup>2+</sup> are  $|c_k|^2$ , and the asymptotic values of these populations are the probabilities for transition to the collision channels. For  $k \neq i$ , they are

$$P_{ik}(v, \mathbf{b}) = \lim_{t \rightarrow \infty} |c_k|^2. \quad (6)$$

The total cross-section for a trajectory orientation is

$$\sigma_{ik}(v) = 2\pi \int_0^\infty b P_{ik}(v, b) db. \quad (7)$$

As mentioned above, our calculation employs potential energy cuts of the potential energy surfaces and non-adiabatic couplings obtained along the projectile trajectories t1, t2, and t3 [21]; the orientation-averaged total cross-section is simply the mean value of the cross-sections obtained with (7) for each trajectory orientation.

To illustrate the collision mechanism, we show in Figure 1 the cut of the electronic energies along a line that forms an angle of 60° with the H–H internuclear axis. Reaction (3) takes place through transitions from the degenerate entrance channels, Sn<sup>2+</sup>(<sup>3</sup>P<sup>o</sup>) + H<sub>2</sub>(X<sup>1</sup>Σ<sub>g</sub><sup>+</sup>), to the capture channels Sn<sup>+</sup>(<sup>2</sup>P<sup>o</sup>) in the neighborhood of the avoided crossings at  $R \approx 7$  a.u. The transitions at inner avoided crossings will populate the molecular state dissociating into Sn<sup>+</sup>(5s5p<sup>2</sup> <sup>4</sup>P) + H<sub>2</sub><sup>+</sup>(X<sup>2</sup>Σ<sub>g</sub><sup>+</sup>). One can note the very narrow avoided crossing between the energy curve of the Sn<sup>+</sup>(<sup>4</sup>P) channel with the curve of the dissociative excitation channel at  $R \approx 9$  a.u. The energy of the ground state, correlating to the entrance channel Sn<sup>2+</sup>(5s<sup>2</sup> <sup>1</sup>S), is very low compared to those of the other electronic states and does not exhibit any avoided crossing.

Figure 2 shows the total cross-sections for Sn<sup>2+</sup> and Sn<sup>2+\*</sup>, for collision energies between 0.3 and 1000 keV. The cross-sections for the individual trajectories t1, t2, and t3, not shown in the figure, differ by less than 10%, which reflects the quasi-isotropy of the projectile–target interaction at the distances where electron capture takes place. It should be noted that the lower part of the energy range, up to roughly 20 keV, is representative for Sn ions ejected from an LPP in an industrial photolithography machine. In this energy range, the cross-sections for metastable Sn<sup>2+\*</sup> are an order of magnitude larger than the ones for ground-state Sn<sup>2+</sup>. Therefore, we focus our attention on Sn<sup>2+\*</sup>, i.e., reaction (3). Due to the endothermic nature of electron capture by ground-state Sn<sup>2+</sup> ions, their contribution only becomes relevant at high collision energies.

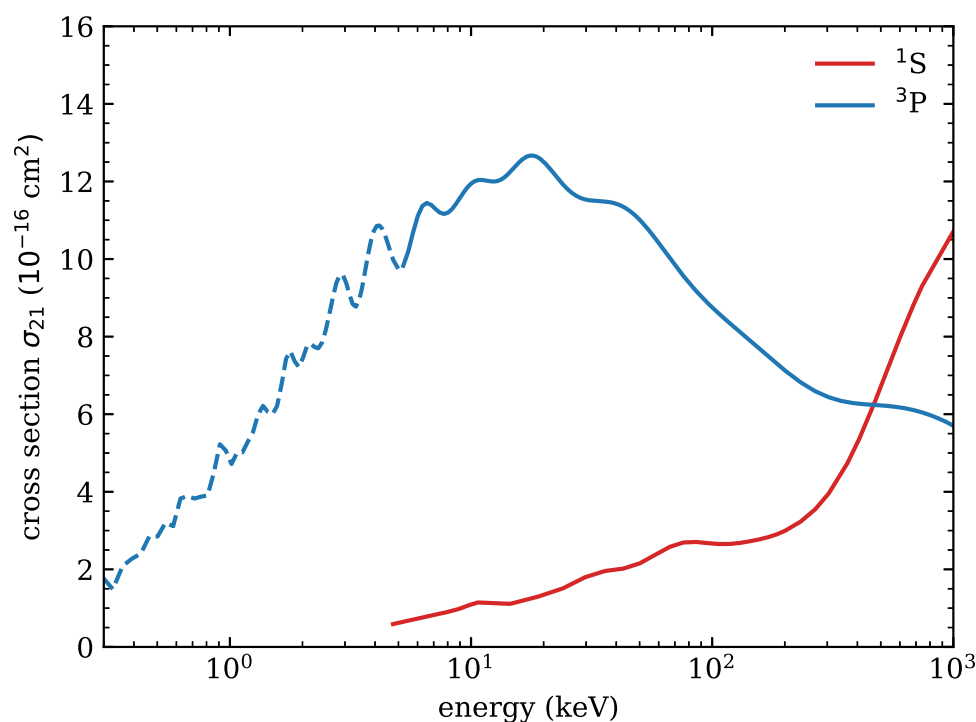


**Figure 2.** Total single-electron capture cross-section in collision of  $\text{Sn}^{2+}$  with  $\text{H}_2$ , as a function of the collision energy, both for ground-state ( $^1\text{S}$ ) and metastable ( $^3\text{P}$ )  $\text{Sn}^{2+}$ . The dashed line shows the extension of the  $^3\text{P}$  calculation to lower energies where vibrational and nuclear quantum effects could be important.

### 3. Experimental Approach

An intuitive experimental approach to measure cross-sections for  $\text{Sn}^{2+}$  and  $\text{Sn}^{2+*}$  would entail generating beams of  $\text{Sn}^{2+}$  ions in the ground ( $5s^2\ ^1\text{S}$ ) and metastable ( $5s5p\ ^3\text{P}^0$ ) state, separately, and measure their change in charge state composition after traversing through a region of  $\text{H}_2$  gas. However, it is very difficult to know and control the metastable fractions in an ion beam [22]. But, as mentioned in the introduction, we do know that in the energy regime relevant for EUV-LPPs,  $\text{Sn}^{3+}$  ions undergoing single-electron capture with  $\text{H}_2$  lead to  $\text{Sn}^{2+}$  ions almost exclusively in the  $5s5p\ ^3\text{P}^0$  term. Therefore, in this work, we use a  $\text{Sn}^{3+}$  ion beam and extract the cross-section for  $\text{Sn}^{2+*}$  from ions that undergo two collisions, capturing one electron each time, i.e.,  $\text{Sn}^{3+} \rightarrow \text{Sn}^{2+*} \rightarrow \text{Sn}^+$ .

Recently, we measured single- and double-electron capture cross-sections for  $\text{Sn}^{3+}$  ions colliding with molecular hydrogen [23], using an upgraded version of the crossed-beam setup used by Rai et al. [15]. The upgrade consists of a deceleration platform and the replacement of the Faraday cup by a retarding field analyzer (RFA), which allows us to measure individual charge states. In the current work, we make use of this upgraded setup. This setup and some parts of the measurement procedure are explained in detail in references [15,23]. Here, the key points will be repeated and new elements of the data analysis procedure will be explained in more detail.

#### 3.1. Experimental Setup

The ZERNIKLEIF facility is used to generate a beam of 21 keV  $\text{Sn}^{3+}$  ions, which is subsequently transported to the crossed-beam setup. The latter is on an elevated potential to decelerate the ions to a desired energy just before entering the collision chamber. A six-element deceleration lens improves transmission. The ion beam traverses a jet of molecular hydrogen flowing from a capillary. Three values of gas flow are used, namely 1, 2.5, and 4 mL/min. These flows are high enough that measurable fractions of the ions undergo

two charge exchange collisions. We are interested in the ions that undergo single-electron capture twice. The ion beam is finally collected and analyzed by an RFA, which provides charge state resolution in the beam current. The next section explains how we extract the cross-section for the second capture event from our measurements.

### 3.2. Measurement Procedure

Starting from a  $\text{Sn}^{3+}$  beam, the relevant processes are described by the following differential equations:

$$\frac{dN^{3+}}{dz} = -(\sigma_{32} + \sigma_{31})nN^{3+} \quad (8a)$$

$$\frac{dN^{2+}}{dz} = \sigma_{32}nN^{3+} - (\sigma_{21} + \sigma_{20})nN^{2+} \quad (8b)$$

$$\frac{dN^{1+}}{dz} = \sigma_{31}nN^{3+} + \sigma_{21}nN^{2+} - \sigma_{10}nN^{1+} \quad (8c)$$

$$\frac{dN^{0+}}{dz} = \sigma_{20}nN^{2+} + \sigma_{10}nN^{1+}, \quad (8d)$$

where  $N^{q+}$  is the number of  $\text{Sn}^{q+}$  ions ( $q = 0, 1, 2, 3$ ) as a function of distance  $z$  through a target of  $\text{H}_2$  gas with number density  $n$ , and  $\sigma_{ij}$  denotes the cross-section for charge exchange from  $\text{Sn}^{i+}$  to  $\text{Sn}^{j+}$ . Note that, with  $N^{2+}$ , we in fact mean the number of  $\text{Sn}^{2+*}$  ions here. Due to the absence of potential-energy curve crossings,  $\sigma_{20} = \sigma_{10} = 0$ , and we can exclude these processes from the analysis. The initial number of ions in the  $\text{Sn}^{3+}$  beam is  $N_0$  and leads to the following initial condition:  $N^{3+}(z = 0) = N_0$ . The analytical solution to the initial value problem is given by the following expressions:

$$N^{3+} = N_0 e^{-(\sigma_{32} + \sigma_{31})nz}, \quad (9a)$$

$$N^{2+} = N_0 \frac{\sigma_{32}}{\sigma_{32} + \sigma_{31} - \sigma_{21}} \left( e^{-\sigma_{21}nz} - e^{-(\sigma_{32} + \sigma_{31})nz} \right), \quad (9b)$$

$$N^{1+} = N_0 \frac{\sigma_{31} - \sigma_{21}}{\sigma_{32} + \sigma_{31} - \sigma_{21}} \left( 1 - e^{-(\sigma_{32} + \sigma_{31})nz} \right) + N_0 \frac{\sigma_{32}}{\sigma_{32} + \sigma_{31} - \sigma_{21}} \left( 1 - e^{-\sigma_{21}nz} \right). \quad (9c)$$

We are interested in so-called double-collision events, which turn a  $\text{Sn}^{2+}$  ion into a  $\text{Sn}^{1+}$  ion by reaction (3). We therefore define the following ratio:

$$f = \frac{N^{1+}}{N^{2+}}, \quad (10)$$

which can be expected to increase with target density due to the occurrence of more double collisions. To see how  $f$  scales with target density, we take a second-order Taylor expansion of Equations (9b) and (9c) and subsequently take the ratio. By ignoring quadratic terms in  $n$  in the resulting expression, we obtain

$$f = \frac{\sigma_{31}}{\sigma_{32}} + \frac{1}{2} \frac{\sigma_{21}(\sigma_{32} + \sigma_{31})}{\sigma_{32}} nz. \quad (11)$$

In our experimental setup, we measure the ion numbers  $N^{q+}$  with the RFA. The position of the RFA in the chamber determines the total length  $L$  over which the ions traverse the molecular target. As in the previous studies [15,23], we make use of the fact that the integral target density  $nL = \int_0^L n(z)dz$  is proportional to the pressure  $P$  in the collision chamber. The constant of proportionality  $\beta$  is determined by calibrating the system with ions of known cross-sections, in this case  $\text{O}^{6+}$  of Ref. [24]. By defining  $f_0 = \frac{\sigma_{31}}{\sigma_{32}}$ , Equation (11) can be rewritten as

$$f = f_0 + \frac{1}{2} \sigma_{21} (1 + f_0) \beta P. \quad (12)$$

In the experiments, we measure the ratio  $f$  at several values of target density, i.e., pressure. Figure 3 shows the results of a typical measurement. It shows that the ratio  $f$  is linear with pressure over our pressure range, justifying the linear approximation of Equation (12). Figure 3 also shows a least-squares linear fit to the data. From the y-intercept ( $f_0$ ) and the slope ( $\frac{df}{dP}$ ), we can determine the cross-section for process (3) using Equation (12):

$$\sigma_{21} = \frac{2 \frac{df}{dP}}{(1 + f_0)\beta}. \quad (13)$$

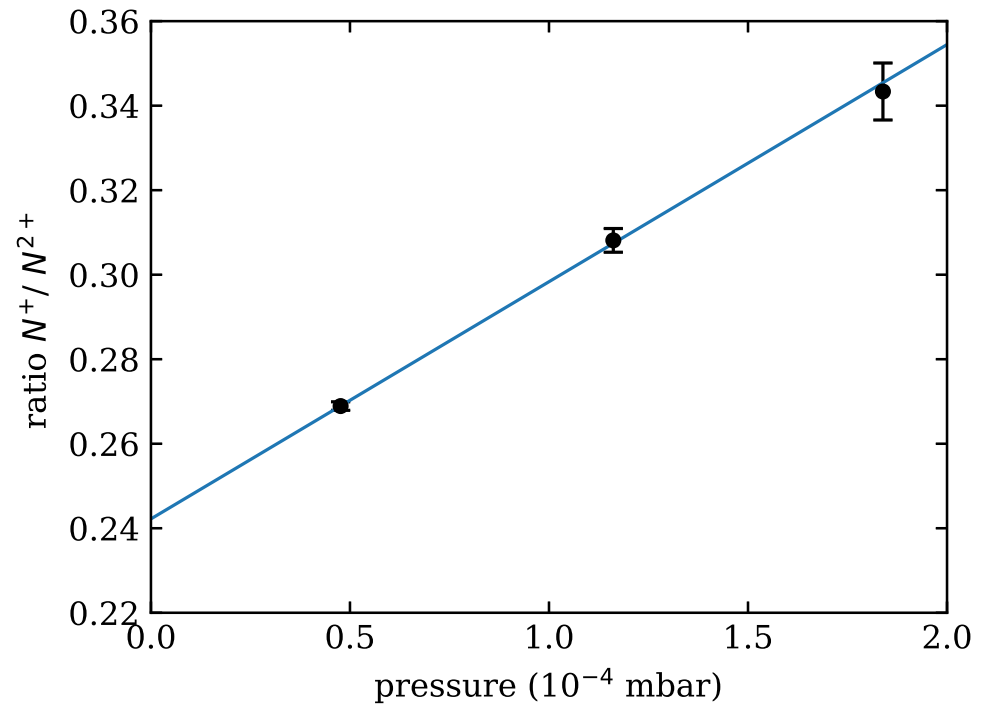


**Figure 3.** Ratio  $N^+/N^{2+}$ , i.e.,  $f$ , measured at three  $H_2$  pressures for incoming  $Sn^{3+}$  ions of 1 keV (black symbols). The blue line is a least-squares linear fit to the data. The resulting y-intercept and slope are used to calculate  $\sigma_{21}$  according to Equation (13).

### 3.3. Uncertainties

The error bars in Figure 3 reflect the statistical uncertainty of one standard deviation in the measurement data. The fitting algorithm translates these into an uncertainty in  $f_0$  and  $\frac{df}{dP}$ , which propagate into a (partial) uncertainty in  $\sigma_{21}$ . Another contribution to the uncertainty in  $\sigma_{21}$  is reproducibility. By repeating measurements on different days and with different ion beam settings, this contribution is found to be 20%. The quadratic sum of both contributions defines the total statistical uncertainty, and is depicted by the error bars plotted in the next section (Figure 4). The systematic uncertainty due to the calibration by the reference data, estimated to be 7%, is not included in the error bars.



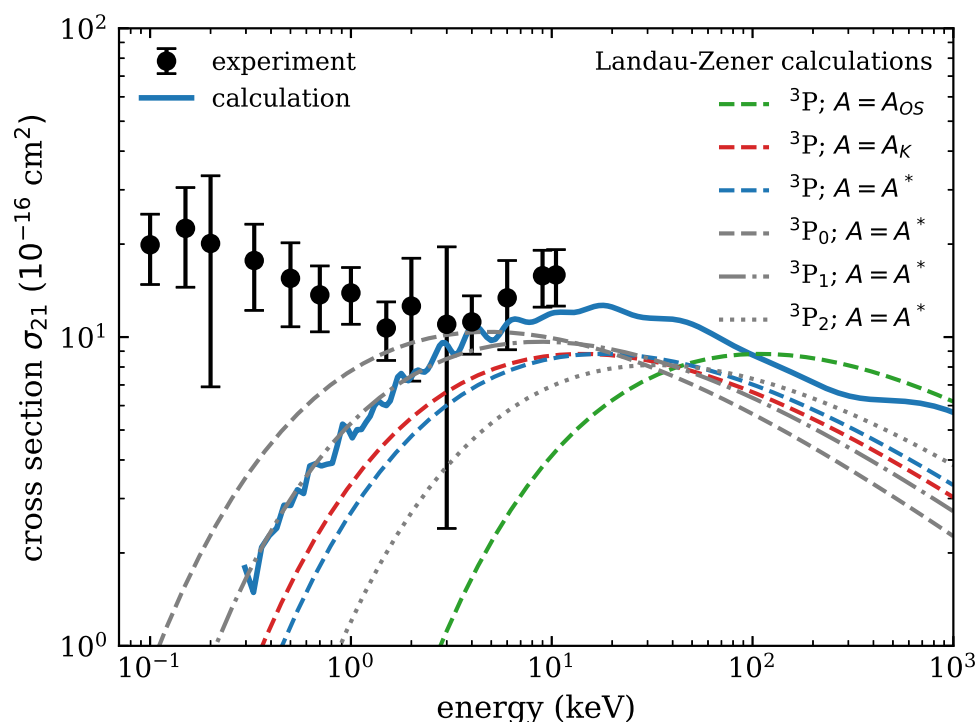


**Figure 4.** Single-electron capture cross-section for  $\text{Sn}^{2+*}(^3P) + \text{H}_2$ . The solid blue line is the result of the semi-classical calculation, and the dots show the experimental results. The dashed green, red, and blue lines show the results of two-state Landau–Zener calculations of the  $^3P$  term, assuming a statistical  $J$  distribution and capture into the  $\nu' = 2$  vibrational state of  $\text{H}_2$ , which has the highest Franck–Condon factor. The green curve uses the prefactor of Olson and Salop [16], and the red curve uses the one from the work by Kimura et al. [17]. The prefactor was varied to match the semi-classical calculation best, resulting in a prefactor of 5.8 and the blue dashed line. This prefactor is subsequently used for Landau–Zener level-calculations, resulting in the light gray curves for  $J = 0, 1, 2$ .

#### 4. Results and Discussion

Figure 4 shows both our calculated and measured cross-sections for  $\text{Sn}^{2+*}$  (reaction (3)). In the energy range from 2 to 10 keV, there is good agreement, while below roughly 2 keV the experimental and calculated values start to diverge. The experimental values show an increasing trend when decreasing the energy down to 0.1 keV.

The entrance channel of the capture process (3) is a mixture of three spectroscopic levels  $^3P_J^o$  with  $J = 0, 1, 2$ , while a single state, representing the  $^3P$  term, has been considered in the non-relativistic theoretical description used in this paper. To determine the effect of the spin-orbit splitting, and to investigate the possibility that a highly  $J$ -dependent cross-section may explain the large experimental cross-sections at low energies, exploratory Landau–Zener calculations were performed. The results are also plotted in Figure 4. First, two-state calculations were performed with the  $^3P$  term as entrance channel, assuming a statistical  $J$  distribution. Following Olson and Salop [16] as well as Magee [25], the coupling matrix element includes the Franck–Condon factor of the most probable vibrational state of  $\text{H}_2^+$ , which is  $\nu' = 2$  [26], to account for the molecular nature of the target. As already mentioned in the introduction, the coupling matrix element has an empirical prefactor  $A$ . Commonly used values are  $A_{OS} = 9.13$  proposed by Olson and Salop [16] and  $A_K = 5.48$  proposed by Kimura et al. [17]. Calculations were performed for both values. Both curves have a similar shape as the semi-classical calculation, but lie roughly 30% lower. The Kimura curve peaks at almost the same energy as the semi-classical curve, whereas the Olson–Salop curve peaks at one order of magnitude higher energy. This means that molecular hydrogen as a target is better approximated by a He atom than by a H atom. We

however choose to optimize the prefactor such that it peaks at exactly the same energy as the semi-classical calculation, and find a value of 5.8, which we denote by  $A^*$ . This prefactor is subsequently used to perform Landau–Zener calculations for the three  $J$  levels. Due to the fact that the spacing between those levels is smaller than the adiabatic splitting, we treat them independently instead of performing multichannel calculations. It can be seen from Figure 4 that the resulting curve for  $J = 0$ , and to a lesser extent also for  $J = 1$ , shifts up and its maximum moves to lower energies. From this, we may conclude that the  $J$ -distribution of the  $^3P$  term is not statistical but has a preference for  $J$  equal to 0 and 1. However, the large experimental cross-sections below 1 keV can still not be explained.

As already mentioned in Section 2, the semi-classical calculation does not take vibrational motion in the  $H_2$  molecule into account. The vibrational period is equal to 8 fs. This should be compared to the interaction time between the projectile and the target. By assuming an interaction distance of 10 a.u., the interaction time of a 1 keV Sn ion is 13 fs, whereas it is 4 fs for a 10 keV Sn ion. This shows that, as the energy decreases from 10 keV, the limits of the applicability of the Franck–Condon approximation begin to be reached. We therefore believe that vibrational effects in the  $H_2$  molecule are responsible for the increase in the cross-section below 1 keV.

## 5. Conclusions

We have performed a joint theoretical and experimental study of single-electron capture by  $Sn^{2+}$  ions from molecular hydrogen. Cross-sections for this process are relevant for ion mitigation simulation codes used for modern EUV photolithography machines. The semi-classical calculations use a close-coupling method on a basis of electronic wavefunctions of the  $(SnH_2)^{2+}$  system and make use of the Franck–Condon approximation (fixed H–H internuclear distance). Consistent with expectations based on binding energies, the calculations show that, at low energies relevant for EUV applications, the cross-section for metastable  $Sn^{2+}(5s5p\ ^3P^o)$  ions ( $Sn^{2+*}$ ) is much larger compared to ground-state  $Sn^{2+}(5s^2\ ^1S)$  ions. The experimental cross-sections for these  $Sn^{2+*}$  ions are extracted from double collisions in a crossed-beam experiment of  $Sn^{3+}$  with  $H_2$ . In the highest part of the overlapping energy range, i.e., from 2 to 10 keV, we find good agreement between calculation and experiment. For lower energies, however, the measured cross-sections increase, whereas the calculated ones decrease. Additional Landau–Zener calculations were performed to investigate the role of the spin–orbit interaction. This interaction has a considerable effect on the cross-sections for the three  $J$  levels; however, it cannot explain the large measured cross-sections at low energies. Since the interaction time becomes larger than the vibrational period of the  $H_2$  molecule for a projectile energy below a few keV, we believe that vibrations become important at those energies. The break-down of the Franck–Condon approximation could be the reason for the discrepancy between theory and experiment at low energies.

**Author Contributions:** Conceptualization, R.H.; methodology, K.B., E.d.W., I.R. and L.M.; software, K.B., L.O., E.d.W. and I.R.; validation, K.B. and E.d.W.; formal analysis, K.B. and E.d.W.; investigation, K.B., L.O., E.d.W., L.A. and I.R.; resources, L.O., L.A., I.R. and R.H.; data curation, K.B. and I.R.; writing—original draft preparation, K.B. and L.M.; writing—review and editing, K.B., L.O., L.A., I.R., L.M. and R.H.; visualization, K.B. and I.R.; supervision, R.H.; project administration, R.H.; funding acquisition, L.M. and R.H. All authors have read and agreed to the published version of the manuscript.

**Funding:** Theoretical research was funded by MINISTERIO DE ECONOMÍA Y COMPETITIVIDAD (Spain), project no. FIS2017-84684-R.

**Data Availability Statement:** The raw data supporting the conclusions of this article will be made available by the authors on request.

**Acknowledgments:** Calculations were performed at the Centro de Computación Científica of UAM. The experimental work was carried out at the ZERNIKELEIF facility in the Zernike Institute for Advanced Materials of the University of Groningen as part of the research portfolio of the Advanced Research Center for Nanolithography (ARCNL), a public–private partnership between the University of Amsterdam (UvA), the Vrije Universiteit Amsterdam (VU), the University of Groningen (RuG), the Netherlands organization for Scientific Research (NWO), and the semiconductor equipment manufacturer ASML.

**Conflicts of Interest:** The authors declare no conflict of interest. The funders had no role in the design of the study; in the collection, analyses, or interpretation of data; in the writing of the manuscript; or in the decision to publish the results.

## References

1. Banine, V.Y.; Koshelev, K.N.; Swinkels, G.H.P.M. Physical processes in EUV sources for microlithography. *J. Phys. D Appl. Phys.* **2011**, *44*, 253001. [[CrossRef](#)]
2. Fomenkov, I.; Brandt, D.; Ershov, A.; Schafgans, A.; Tao, Y.; Vaschenko, G.; Rokitski, S.; Kats, M.; Vargas, M.; Purvis, M.; et al. Light sources for high-volume manufacturing EUV lithography: Technology, performance, and power scaling. *Adv. Opt. Technol.* **2017**, *6*, 173. [[CrossRef](#)]
3. Bakshi, V. (Ed.) *EUV Lithography*, 2nd ed.; SPIE Press: Bellingham, WA, USA, 2018.
4. Svendsen, W.; O’Sullivan, G. Statistics and characteristics of xuv transition arrays from laser-produced plasmas of the elements tin through iodine. *Phys. Rev. A* **1994**, *50*, 3710–3718. [[CrossRef](#)] [[PubMed](#)]
5. O’Sullivan, G.; Li, B.; D’Arcy, R.; Dunne, P.; Hayden, P.; Kilbane, D.; McCormack, T.; Ohashi, H.; O’Reilly, F.; Sheridan, P.; et al. Spectroscopy of highly charged ions and its relevance to EUV and soft x-ray source development. *J. Phys. B At. Mol. Opt. Phys.* **2015**, *48*, 144025. [[CrossRef](#)]
6. Colgan, J.; Kilcrease, D.; Abdallah, J.; Sherrill, M.; Fontes, C.; Hakel, P.; Armstrong, G. Atomic structure considerations for the low-temperature opacity of Sn. *High Energy Density Phys.* **2017**, *23*, 133–137. : 10.1016/j.hedp.2017.03.009 [[CrossRef](#)]
7. Versolato, O.O. Physics of laser-driven tin plasma sources of EUV radiation for nanolithography. *Plasma Sources Sci. Technol.* **2019**, *28*, 083001. [[CrossRef](#)]
8. Torretti, F.; Sheil, J.; Schupp, R.; Basko, M.; Bayraktar, M.; Meijer, R.; Witte, S.; Ubachs, W.; Hoekstra, R.; Versolato, O.; et al. Prominent radiative contributions from multiply-excited states in laser-produced tin plasma for nanolithography. *Nat. Commun.* **2020**, *11*, 2334. [[CrossRef](#)] [[PubMed](#)]
9. Fujioka, S.; Nishimura, H.; Nishihara, K.; Murakami, M.; Kang, Y.G.; Gu, Q.; Nagai, K.; Norimatsu, T.; Miyanaga, N.; Izawa, Y.; et al. Properties of ion debris emitted from laser-produced mass-limited tin plasmas for extreme ultraviolet light source applications. *Appl. Phys. Lett.* **2005**, *87*, 241503. [[CrossRef](#)]
10. Poirier, L.; Bayerle, A.; Lassise, A.; Torretti, F.; Schupp, R.; Behnke, L.; Mostafa, Y.; Ubachs, W.; Versolato, O.O.; Hoekstra, R. Cross-calibration of a combined electrostatic and time-of-flight analyzer for energy-and charge-state-resolved spectrometry of tin laser-produced plasma. *Appl. Phys. B* **2022**, *128*, 39. [[CrossRef](#)]
11. Rai, S.; Bijlsma, K.I.; Poirier, L.; de Wit, E.; Assink, L.; Lassise, A.; Rabadán, I.; Méndez, L.; Sheil, J.; Versolato, O.O.; et al. Evidence of production of keV Sn<sup>+</sup> ions in the H<sub>2</sub> buffer gas surrounding an Sn-plasma EUV source. *Plasma Sources Sci. Technol.* **2023**, *32*, 035006. [[CrossRef](#)]
12. Burdt, R.A.; Ueno, Y.; Tao, Y.; Yuspeh, S.; Tillack, M.S.; Najmabadi, F. Recombination effects during expansion into vacuum in laser produced Sn plasma. *Appl. Phys. Lett.* **2010**, *97*, 041502. [[CrossRef](#)]
13. Nakamura, D.; Tamaru, K.; Hashimoto, Y.; Okada, T.; Tanaka, H.; Takahashi, A. Mitigation of fast ions generated from laser-produced Sn plasma for extreme ultraviolet light source by H<sub>2</sub> gas. *J. Appl. Phys.* **2007**, *102*, 123310. [[CrossRef](#)]
14. Abramenko, D.B.; Spiridonov, M.V.; Krainov, P.V.; Krivtsun, V.M.; Astakhov, D.I.; Medvedev, V.V.; van Kampen, M.; Smeets, D.; Koshelev, K.N. Measurements of hydrogen gas stopping efficiency for tin ions from laser-produced plasma. *Appl. Phys. Lett.* **2018**, *112*, 164102. [[CrossRef](#)]
15. Rai, S.; Bijlsma, K.I.; Rabadán, I.; Méndez, L.; Wolff, P.A.J.; Salverda, M.; Versolato, O.O.; Hoekstra, R. Charge exchange in collisions of 1–100-keV Sn<sup>3+</sup> ions with H<sub>2</sub> and D<sub>2</sub>. *Phys. Rev. A* **2022**, *106*, 012804. [[CrossRef](#)]
16. Olson, R.E.; Salop, A. Electron transfer between multicharged ions and neutral species. *Phys. Rev. A* **1976**, *14*, 579. [[CrossRef](#)]
17. Kimura, M.; Iwai, T.; Kaneko, Y.; Kobayashi, N.; Matsumoto, A.; Ohtani, S.; Okuno, K.; Takagi, S.; Tawara, H.; Tsurubuchi, S. Landau-Zener model calculations of one-electron capture from He atoms by highly stripped ions at low energies. *J. Phys. Soc. Jpn.* **1984**, *53*, 2224–2232. [[CrossRef](#)]
18. Barragán, P.; Errea, L.F.; Méndez, L.; Rabadán, I.; Riera, A. Electron capture in collisions of N<sup>2+</sup> and O<sup>2+</sup> ions with H(1s) at low impact energies. *Phys. Rev. A* **2006**, *74*, 024701. [[CrossRef](#)]
19. Schneiderman, S.B.; Russek, A. Velocity-Dependent Orbitals in Proton-On-Hydrogen-Atom Collisions. *Phys. Rev.* **1969**, *181*, 311–321. [[CrossRef](#)]
20. Errea, L.F.; Gorfinkiel, J.D.; Macías, A.; Méndez, L.; Riera, A. Implementation of the sudden approximation eikonal method in ion-diatom collisions. *J. Phys. B At. Mol. Opt. Phys.* **1997**, *30*, 3855. [[CrossRef](#)]

21. Rabadán, I.; Méndez, L. Orientation effects in ion-molecule collisions. *J. Phys. Conf. Ser.* **2017**, *875*, 012009. [[CrossRef](#)]
22. Welton, R.F.; Moran, T.F.; Thomas, E.W. Metastable state abundances in multiply charged ion beams. *J. Phys. B At. Mol. Opt. Phys.* **1991**, *24*, 3815. [[CrossRef](#)]
23. Bijlsma, K.; Assink, L.; Oltra, L.; Rabadán, I.; de Wit, E.; Kleinsmit, A.; Lalkens, E.; Salverda, M.; Versolato, O.O.; Méndez, L.; et al. Single and double electron capture in low-energy collisions of Sn<sup>3+</sup> ions with molecular hydrogen. 2024, *in preparation*.
24. Machacek, J.R.; Mahapatra, D.P.; Schultz, D.R.; Ralchenko, Y.; Chutjian, A.; Simcic, J.; Mawhorter, R.J. Measurement and calculation of absolute single- and double-charge-exchange cross sections for O<sup>6+</sup> ions at 1.17 and 2.33 keV/u impacting He and H<sub>2</sub>. *Phys. Rev. A* **2014**, *90*, 052708. [[CrossRef](#)]
25. Magee, J.L. Charge neutralization by reaction between positive and negative ions. *Discuss. Faraday Soc.* **1952**, *12*, 33–44. [[CrossRef](#)]
26. Wacks, M. Franck-Condon factors for ionization of H<sub>2</sub>, HD and D<sub>2</sub>. *J. Res. Natl. Bur. Stand. Sect. A* **1964**, *68*, 631–633. [[CrossRef](#)] [[PubMed](#)]

**Disclaimer/Publisher's Note:** The statements, opinions and data contained in all publications are solely those of the individual author(s) and contributor(s) and not of MDPI and/or the editor(s). MDPI and/or the editor(s) disclaim responsibility for any injury to people or property resulting from any ideas, methods, instructions or products referred to in the content.